Emergence of spatial order in highly interacting Rydberg gases

João D. Rodrigues,[1,2,*] Hugo Terças,[1] Luis F. Gonçalves,[2] Luis G. Marcassa,[2] and José T. Mendonça[1]
[1]*Instituto de Plasmas e Fusão Nuclear, Instituto Superior Técnico, Universidade de Lisboa, 1049-001 Lisbon, Portugal*
[2]*Instituto de Física de São Carlos, Universidade de São Paulo, Caixa Postal 369, 13560-970, São Carlos, São Paulo, Brazil*

(Received 9 August 2017; published 22 February 2018)

We describe the emergence of strong spatial correlations, akin to liquidlike behavior and crystallization effects, in low- (one- and two-)dimensional gases of cold Rydberg atoms. The presence of an external electric field permanently polarizes the atoms, which became highly correlated due to the long-range dipole-dipole interaction. We describe a theoretical approach particularly suited for strongly coupled systems and numerically obtain both the two-particle distribution function and the static structure factor. The experimental implementation of such highly interacting systems is discussed, including detailed calculations of the interaction strength for different Rydberg states. The results provide insights into many-body effects associated with strongly interacting Rydberg atoms, including the possibility of observing highly ordered phases.

DOI: 10.1103/PhysRevA.97.022708

I. INTRODUCTION

Rydberg atoms [1,2] provide a powerful platform to study strongly interacting systems. One manifestation of such interactive character is the so-called blockade effect, where Rydberg states strongly inhibit further excitation of their neighbors, either due to van der Waals [3,4] or dipole-dipole interactions [5,6], which has been exploited, for instance, in the implementation of quantum gates for information processing [7]. Moreover, the interactions between the high-lying electronic states can be mapped onto light fields, giving rise to strong nonlinear optical effects (photon-photon interactions) [8,9], even at the single-photon level [10], allowing for the storage and manipulation of quantum optical states in highly excited collective states (Rydberg polaritons) [11]. Moreover, the combination of the strong interactive character with the easy manipulation of Rydberg states constitutes an ideal approach for quantum simulation [12,13] and general many-body physics [14,15].

Here, we describe a rather distinct manifestation of the interactive character of Rydberg atoms, namely, the emergence of strong spatial correlations in low-dimensional gases. While many studies have been dedicated to the dynamics and transport of Rydberg excitations [12,13,16–18], in the so-called frozen gas regime, the investigation of the external (motional) degrees of freedom has received less attention. Among the few counterexamples [19–21], recent studies [22–26] have demonstrated, however, that Rydberg gases are suitable to the study of the (motional) dynamics associated with highly correlated particle systems, a problem which has been subject to extensive theoretical, computational, and experimental research [27–34]. Using integral equation techniques and surpassing the need to resort to molecular dynamics simulations, we are able to describe the emergence and nature of spatial correlations, in a wide range of coupling parameters, defined as the ratio of potential to kinetic (thermal) energy, from weakly to strongly correlated regimes. We begin by introducing the integral equation approach for a low-dimensional Rydberg gas under dipole-dipole interactions, and obtain both the two-particle distribution function and the structure factor. The results are analyzed in detail and routes towards the experimental obtainment of such highly interacting Rydberg systems are discussed, together with numerical calculations of the coupling parameter for different states.

II. THEORY

In a permanently polarized sample, Rydberg atoms interact via the general dipole-dipole potential [24,35–37],

$$V(r,\theta) = \frac{C_3}{r^3}[1 - 3\cos^2(\theta)], \tag{1}$$

with θ the angle between the interatomic separation vector $\mathbf{r}$ and the atomic dipoles $\mathbf{P}$ (aligned with external electric field $\mathbf{E}_0$). The strength of the interaction is quantified by $C_3 = P^2/4\pi\epsilon_0$, with P the atomic dipole moment and ϵ_0 the vacuum electric permittivity. In a one-dimensional sample, the character of the interaction (attractive or repulsive) depends on the polarization angle. In particular, there exists a magic angle $\theta = 54.7^\circ$ such that the interatomic potential vanishes [38]. In a two-dimensional gas, an isotropic repulsive interaction is obtained when the polarization is perpendicular to the atomic sample. In this case, $\theta = \pi/2$ and the in-plane potential is simply given by $V(r) = C_3/r^3$. The average interparticle distance in a two-dimensional sample is defined as $a = (\pi n_0)^{-1/2}$, with $n_0 = 1/\pi$ the homogeneous density, in units of r/a. The coupling coefficient may be defined as the mean ratio between potential and kinetic energy, $\Gamma = \langle V(r)\rangle/k_BT$, with k_B the Boltzmann constant and T the temperature of the gas, and in terms of the mean interparticle distance $\Gamma = C_3/k_BTa^3$. The weakly and highly correlated regimes, $\Gamma \ll 1$ and $\Gamma \gg 1$, respectively, shall be addressed here.

In general, the (classical) description of strongly coupled systems falls outside the scope of hydrodynamical or

*Corresponding author: joaodmrodrigues@tecnico.ulisboa.pt

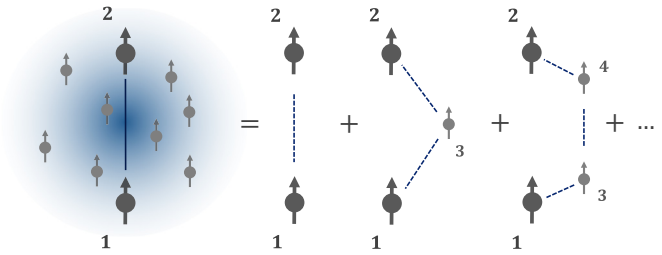

FIG. 1. Schematic illustration of the origin of correlation between any pair of dipoles (Rydberg atoms). Besides the direct correlation between 1 and 2, indirect correlations mediated by any number of intermediate particles must be taken into account.

Vlasov-like formulations for single-particle densities, where correlations between the atoms are usually ignored. Nevertheless, even in the presence of strong correlations and for conditions of thermal equilibrium, the full N-particle density, $\rho^{(N)}(\mathbf{r}^N)$, can be truncated to lower orders, introducing the single- and the two-particle functions [39], $\rho^{(1)}(\mathbf{r}) = \langle \sum_i \delta(\mathbf{r}-\mathbf{r}_i)\rangle$ and $\rho^{(2)}(\mathbf{r},\mathbf{r}') = \langle \sum_i \sum_{j\neq i} \delta(\mathbf{r}-\mathbf{r}_i)\delta(\mathbf{r}'-\mathbf{r}_j)\rangle$, respectively, where the summations are taken over the total N particles and averaging over the canonical ensemble, relevant for low fluctuations in the number of atoms. We may safely take the single-particle density as $\rho^{(1)}(\mathbf{r}) = n_0$ and define the (normalized) two-particle distribution $g^{(2)}(\mathbf{r}_1,\mathbf{r}_2) = \rho^{(2)}(\mathbf{r}_1,\mathbf{r}_2)/n_0^2$. In the case of isotropic interactions, $g^{(2)}(\mathbf{r}_1,\mathbf{r}_2) = g^{(2)}(|\mathbf{r}_1-\mathbf{r}_2|) \equiv g(r)$, with the latter usually known as the radial distribution function, such that the average number of particles lying between r and $r+dr$ away from a reference atom is $n_0 g(r)dr$ and $2\pi r n_0 g(r)dr$ in one and two-dimensional samples, respectively. The emergence of correlation, corresponding to $g(r)\neq 1$, or $h(r)\neq 0$, with $h(r) = g(r)-1$ the pair-correlation function, will be fully rooted in the interactions among the Rydberg atoms.

The description of the gas in reciprocal space becomes useful in a number of situations and, in this context, the (static) structure factor is defined as

$$S(\mathbf{k}) = \frac{1}{N}\langle \rho^{(1)}(\mathbf{k})\rho^{(1)}(-\mathbf{k})\rangle = 1 + \frac{1}{N}\left\langle \sum_{i\neq j} e^{-i\mathbf{k}\cdot(\mathbf{r}_i-\mathbf{r}_j)}\right\rangle. \tag{2}$$

The last term in Eq. (2) vanishes when the relative position between any pair of particles, $\mathbf{r}_i-\mathbf{r}_j$, is statistically independent, corresponding to the absence of correlation as $S(\mathbf{k})=1$. Moreover, the static structure factor is related with the radial distribution function by

$$S(k) - 1 = n_0 \int d\mathbf{r} e^{-i\mathbf{k}\cdot\mathbf{r}}[g(r)-1], \tag{3}$$

or, equivalently, $S(k) = 1 + n_0 h(k)$. It directly describes how materials scatter radiation and, without direct-imaging techniques, is usually measured by x-ray or neutron-diffraction experiments. It became instrumental in the study of the internal structure of systems such as liquid helium [40–42] or strongly correlated plasmas [27,43].

The total correlation between two Rydberg atoms arises both from the direct interaction between them and those with intermediate atoms; see Fig. 1. In this context, we may introduce the direct correlation function $c(r)$, related with the total correlation $h(r)$ by the Ornstein-Zernike relation,

$$h(r) = c(r) + n_0 \int d\mathbf{r}' c(|\mathbf{r}-\mathbf{r}'|)h(r'). \tag{4}$$

While the range of $c(r)$ is usually comparable with that of the pair potential $V(r)$, the total correlation function is, in general, of higher range due to the effects of indirect correlations. Although the Ornstein-Zernike (OZ) relation gives an exact relation between the total and direct correlation functions, in order to compute these quantities in a self-consistent manner, some sort of closure condition is needed.

In the absence of drift, pressure and electrostatic forces must balance, $\nabla\phi = -\frac{\nabla p}{n}$, with $\phi(r)$ the potential created by a distribution of Rydberg atoms. For an ideal gas at thermal equilibrium, $p = nk_BT$ and $\nabla[\phi + k_BT\ln(n)] = 0$. The solution $n(r) = n_0\exp[-\phi(r)/k_BT]$ is known as the barometric law, which simply determines the distribution around a test particle in the presence of interactions according to a Boltzmann law. Here, an appropriate potential accounting for both the effects of direct and indirect interactions can be obtained by constructing a hierarchy similar to the OZ relation, where the total potential $\phi(r)$ is the sum of the direct pairwise term $V(r)$ and the indirect contribution from any number of intermediate atoms, namely,

$$\begin{aligned} -\frac{\phi(r)}{k_BT} &= -\frac{V(r)}{k_BT} + n_0\int d\mathbf{r}' c(|\mathbf{r}-\mathbf{r}'|)h(r') \\ &= -\frac{V(r)}{k_BT} + h(r) - c(r), \end{aligned} \tag{5}$$

where the last equality follows from the OZ relation. Evoking the barometric law finally yields

$$g(r) = \exp\left[-\frac{V(r)}{k_BT} + h(r) - c(r)\right]. \tag{6}$$

The latter is known as the hypernetted chain (HNC) closure relation. Together with the OZ relation in Eq. (4), it forms a closed set of equations for the total and direct correlation functions, $h(r)$ and $c(r)$, respectively. We should stress that while the OZ relation is exact, the HNC closure constitutes an approximation rooted at the barometric assumption, performing particularly well for systems displaying long-range interactions.

III. SPATIAL CORRELATIONS

The obtainment of the radial distribution function $g(r)$ implies a numerical approach to the coupled OZ and HNC closure equations. The former becomes more easily expressed in reciprocal space, $h(k) = c(k) + n_0 c(k)h(k)$. For implementation purposes, the indirect correlation function shall be defined as $e(r) = h(r) - c(r)$. The algorithm begins with an initial guess for the direct correlation function, $c_0(r)$. From its Fourier transform $c_0(k)$, we compute the indirect correlation function $e_0(k)$, using the OZ relation in reciprocal space. Finally, from its inverse Fourier transform $e_0(r)$, together with the HNC closure equation, we compute the updated direct correlation function $c_1(r)$ and repeat the entire procedure until convergence is obtained. In general, such numerical scheme is numerically unstable and, to mitigate this effect, we only mix a small part of the new direct correlation function into the old one.

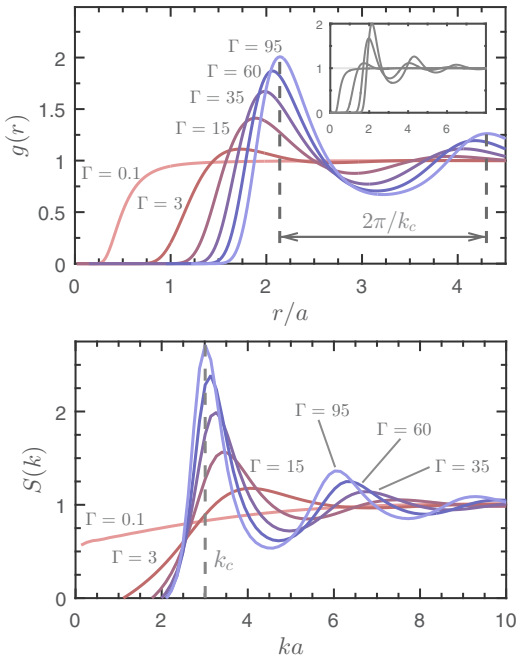

FIG. 2. Two-dimensional Rydberg gas. Top: Radial distribution function for different values of the coupling parameter, displaying the emergence of liquid and quasiperiodic correlations, with k_c the wave number associated with such regularity in the spatial arrangement. The inset plot depicts the oscillatory character of $g(r)$ and the high range persistence of the spatial correlations. Bottom: Static structure factor for different values of Γ. The developing peak at approximately $k_c = 2\pi/\lambda_c \simeq 3a^{-1}$ entails the emergence of stronger correlations and the short-range oscillatory behavior of the radial distribution function.

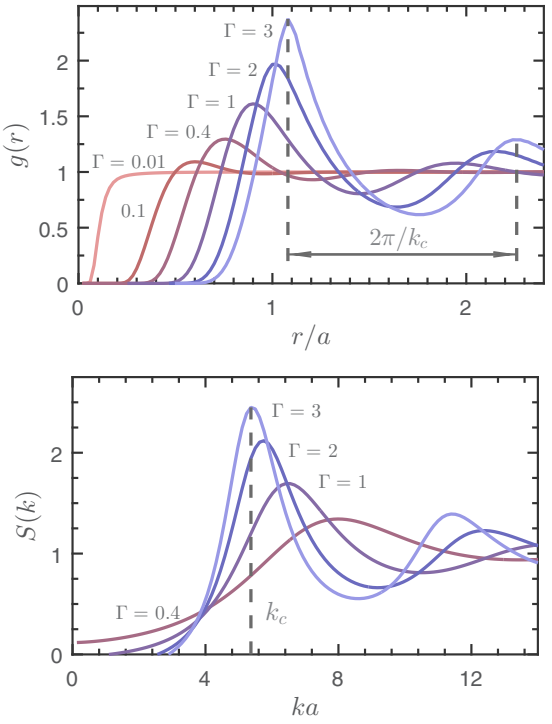

FIG. 3. One-dimensional Rydberg gas. The radial distribution function and static structure factor are depicted in the top and bottom panels, respectively, for different values of Γ. Strong spatial correlations emerge at weaker coupling due to the reduced dimensionality.

The results for a two-dimensional gas are depicted in Fig. 2. For weak correlations, $\Gamma \ll 1$, the only prominent feature is the absence of Rydberg atoms close to the reference particle, located at $r = 0$, due to the repulsive character of the dipole-dipole interaction. For higher values of the coupling parameter, however, we observe the emergence of strong spatial correlations. Besides the greater region of atom depletion near $r = 0$, due to stronger repulsion, a prominent density peak appears located at approximately twice the mean interparticle distance, $r \sim 2a$, followed by successive regions of depletion and accumulation of Rydberg atoms, regularly spaced by approximately $\lambda_c \simeq 2a$. Such oscillatory behavior of $g(r)$ is characteristic of highly correlated systems [27] and entails the crossover between liquid and crystallinelike behavior, associated with the highly interactive character of the system emerging at higher values of Γ [29,30,33]. The emergence of such a highly ordered configuration is also visible in the behavior of the static structure factor, with the growing peaks at multiples of approximately $k_c \simeq 2\pi/\lambda_c$.

In one-dimensional systems, we observe the same kind of spatial order emerging for stronger coupled systems; see Fig. 3. Here, however, lower interaction strengths are required to observe similar configurations due to the reduced degrees of freedom available for spatial arrangement. In other words, the reduced dimensionality makes it harder to create disorder in the system. In fact, no major overhead of interaction-induced ordering to thermal-induced disordering is required to observe the emergence of strong spatial correlations, which begin to appear for much lower values of Γ, of the order of 1. A worthy observation is related to the long-range character of the emerging order. Particularly for the one-dimensional case, the height of the first peak in the radial distribution function grows faster than those of higher order. This essentially means that the dipole-dipole interactions are at the origin of short- to medium-range order, while true long-range order does not fully arise. This kind of behavior is partially explained by the Mermin-Wagner theorem of statistical physics, which essentially states that for $d \leqslant 2$, with d the dimensionality of the system, low momenta thermal fluctuations destroy true long-range order [44,45]. It is also worth mentioning that strongly interacting dipolar gases have been previously investigated in the context of polar molecules [46], with quantum Monte Carlo simulations describing the different ground-state phases, emerging at high densities and temperature close to 1 μK. Here, however, and due to the higher temperatures and lower densities inherent to the Rydberg blockade effect, we describe how dipole-dipole interactions are at the origin of strong correlations and many-body dynamics at the classical level.

IV. EXPERIMENTAL CONSIDERATIONS

Experimentally, the excitation of Rydberg atoms usually relies on a two-photon transition. For ^{85}Rb, the $5S_{1/2}$ ground state is excited to the intermediate $5P_{3/2}$ and subsequently promoted to a high-lying Rydberg level $nS_{1/2}$, for instance. An initial low interacting state ensures small interatomic separations due to blockade effects. For $nS_{1/2}$ levels, the

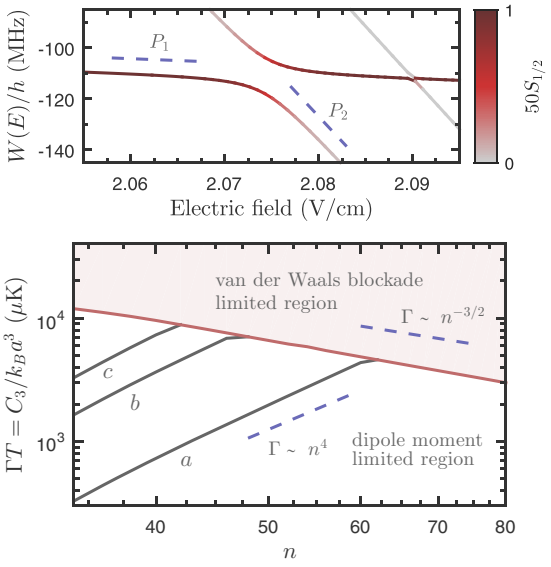

FIG. 4. Top: First avoided crossing in the Stark map for the $50S_{1/2}$ state of ^{85}Rb, whose energy at zero field defines the axis origin. Here, P_1 and P_2 correspond to states of low and high dipolar character, respectively, and the colored lines indicate the amount of $50S_{1/2}$ character. Bottom: Coupling parameter (normalized to the temperature) as a function of n. The a, b, and c (black) curves correspond to a ground-state density (or Rydberg density, by construction) of $n_g = 10^9, 5 \times 10^9$, and 10^{10} cm^{-3}, respectively, where the interaction is limited by the strength of the dipole moment. The red curve depicts the regime limited by the van der Waals blockade, where an on-resonance excitation has been considered, with laser linewidth $\Delta = 3$ MHz.

blockade effect only arises from the weaker van der Waals (repulsive) interaction, which becomes significant only for higher n (principal quantum number). Moreover, for S orbitals, the van der Waals interaction does not depend on the relative atomic orientation, providing fairly homogeneous Rydberg samples. In order to switch into an highly interacting regime, the atoms are transferred to high dipolar states through a Landau-Zener adiabatic passage, promoted by an electric field sweep through an avoided crossing in the Stark landscape [47,48]; see Fig. 4. The final highly dipolar linear Stark state becomes permanently polarized in the direction of the electric field, efficiently transferring the atoms from a low to a highly interacting regime [24,25]. The permanent dipole moment of a state with energy $W(E)$, with E the electric field, is given by the slope $P = -\frac{dW(E)}{dE}$ and, therefore, large dipole-dipole interactions are achieved by exciting Rydberg levels with large slopes in the Stark map.

While the dipole moment quantifies the strength of the interaction, $C_3 = P^2/4\pi\epsilon_0$, another equally important parameter for achieving highly coupled samples is the average interatomic separation a and, here, two regimes can be distinguished. On the one hand, for high ground-state densities and/or high principal quantum number, the van der Waals blockade will limit the Rydberg density. In particular, $V_{\mathrm{vdW}} = C_6/r^6$, with the interaction strength smoothly scaling as $C_6 \propto n^{11}$ [36]. In the case of on-resonance excitation, the blockade radius is such that $\Delta = C_6/r_{\mathrm{B}}^6$, with Δ the linewidth of the excitation laser. In this regime, the average interatomic distance is then limited by the blockade, $a = r_{\mathrm{B}}$. For the sake of reference, $r_{\mathrm{B}} = 2.6$, 4.2, and 6.0 μm, for $n = 40$, 50, and 60, respectively, for the $nS_{1/2}$ states of ^{85}Rb (assuming $\Delta = 3$ MHz). On the other hand, for low principal quantum number and ground-state densities n_g, such that $a = \langle r \rangle = (3/4\pi n_g)^{1/3} > r_{\mathrm{B}}$, with $\langle r \rangle$ the average ground-state interatomic distance, the van der Waals blockade plays no role and the interaction strength will mostly be limited by the magnitude of the permanent dipole moment.

The coupling parameter Γ computed for different principal quantum numbers and normalized to the temperature is depicted in Fig. 4. Here, the atomic dipole moment is computed for the adiabatic state after the first avoided crossing appearing in the Stark map, obtained by diagonalization of the interaction Hamiltonian. In lowest order, the energy shifts from the linear Stark effect scale as $W \propto En^2$ and, consequently, the dipole moment $P \propto n^2$ [36]. In the dipole moment limited regime, where a does not scale with the principal quantum number, $\Gamma \propto P^2 \propto n^4$, which is verified by the numerical results. In the van der Waals blockade regime, however, the scaling of the average interatomic distance (blockade radius) with n must be taken into account. Since $C_6 \propto n^{11}$ and, consequently, $r_{\mathrm{B}} \propto n^{11/6}$, the coupling coefficient $\Gamma \propto n^{-3/2}$, which is also in agreement with the results. Here, the computation of C_6 is performed via second-order perturbation theory. Clearly, the fast increase of the blockade radius is more dramatic then the higher dipole moments and, in this regime, the interaction strength decreases with n.

Notice that immediately after the excitation stage, no particular order is expected in the system. This highly out-of-equilibrium initial state shall be followed by a rapid reorganization of the atomic dipoles. This is accompanied by a fast increase in the temperature of the system, as the randomly positioned dipoles are accelerated by the potential landscape into an equilibrium distribution. This mechanism of disorder-induced heating has been reported in experiments on ultracold neutral plasmas (UCNPs) [49] and could eventually impose a limitation on the achievement of high values of Γ. In the context of UCNPs, it has been demonstrated that the excitation of initially ordered samples greatly reduces the effects associated with disorder-induced heating. This could be obtained either via the Rydberg blockade mechanism [50], where an initial sample of spatially ordered Rydberg atoms is posteriorly ionized, or via the preordering of atoms in a partially filled optical lattice [51]. While the latter could also be employed in the present context, the former more simply means that an initial excitation where the interatomic distance is limited by the blockade mechanism would also suppress the effects associated with disorder-induced heating. As recently demonstrated in [24], a Landau-Zener adiabatic crossing is appropriate to create highly interacting samples, with the emergence of the associated spatial correlations and ordered states occurring in just a few microseconds, much faster than the typical lifetimes of the excited states or collisional processes.

At this point, one could wonder about the nature of the emerging correlations and, in particular, if this rapid forming order entails a state of thermal equilibrium, such that direct comparison with the present results could be performed. Formally, relaxation into thermal equilibrium is usually determined by a Fokker-Planck equation [52], where diffusion

spreading in momentum space is counterbalanced by velocity damping due, in this case, to dipole-dipole interactions. The latter also quantifies the relaxation time τ as the inverse of the rate of velocity change due to dipole interactions. A rough estimate can be performed as $\tau \sim v_{th}/a_d$ [53], with $v_{th} = \sqrt{k_B T/m}$ the thermal speed and a_d the acceleration due to dipole forces. Equivalently, we can write in terms of the coupling coefficient Γ, $\tau \sim a/v_{th}\Gamma = a\sqrt{m/k_B T}/\Gamma$, with a the mean interparticle distance, as defined before. For a sample of ^{85}Rb at a temperature of 100 μK, with $a \sim 2$ μm and a coupling coefficient $\Gamma \sim 10$, such as reported in [24], we obtain a relaxation time $\tau \sim 2$ μs, in excellent agreement with the time scale at which the authors observe the emergence of spatial correlations. This strongly suggests that the observed order corresponds to a state approaching thermal equilibrium as described by the present model.

The experimental obtainment of correlation functions involves the detection of the atomic trajectories. Ion-imaging-based methods proved to be very efficient in this regard for three-dimensional (3D) [54,55] and 1D [25] systems, for both weak van der Waals [23] and strong dipole-dipole [24] interactions. It allows the retrieval of the spatial distribution of Rydberg atoms, with micrometer resolution and single-atom detection capability. The creation of 1D samples can be done by trapping the atoms in a tightly focused dipole trap [25], while, for the 2D case, an astigmatic excitation beam, created by a cylindrical lens, can be used to create a plane of light in the excitation process.

V. CONCLUSION

In summary, we demonstrated the emergence of highly correlated structural phases in low-dimensional gases of Rydberg atoms with strong dipole-dipole interactions. The integral equation technique employed here constitutes a general approach to strongly correlated particle systems, particularly well suited for long-range interactions. Moreover, it surpasses the necessity to resort to other commonly used massive numerical approaches, such as Monte Carlo or molecular dynamics techniques, together with providing easy manipulation of interaction strengths and overall parameter dependences. In the context of Rydberg gases, it can be applied to different kinds of atom-atom interactions, such as van der Waals or soft-core potentials, the latter corresponding to the case of dressing from far off-resonant excitation, where ground-state atoms acquire partial Rydberg character [9,56–58]. Moreover, and contrary to other highly correlated systems, such as liquids, solid-state materials, plasmas, etc., cold (Rydberg) atom experiments benefit from the high degree of control over parameters such as interacting strength or sample dimensionality. As such, together with the results presented here, we argue that Rydberg atoms provide an ideal platform for the investigation of strongly correlated media and many-body physics, opening a route towards the simulation of complex systems with cold-atom experiments [12,13,15,59,60], as well as probing out-of-equilibrium dynamics in strongly interacting systems.

ACKNOWLEDGMENTS

J.D.R. acknowledges the financial support of FCT - Fundação da Ciência e Tecnologia (Portugal) through Grant No. SFRH/BD/52323/2013. H.T. thanks the Security of Quantum Information Group for their hospitality and for partially providing the working conditions, and is thankful for the support from FCT - Fundação da Ciência e Tecnologia (Portugal) through Grant No. IF/00433/2015. This work was partially supported by São Paulo Research Foundation (FAPESP) Grants No. 2011/22309-8 and No. 2013/02816-8, the US Army Research Office Grant No.W911NF-15-1-0638, and CNPq.

[1] T. F. Gallagher, *Rydberg Atoms* (Cambridge University Press, Cambridge, 1994).
[2] L. G. Marcassa and J. P. Shaffer, Adv. At. Mol. Opt. Phys. **63**, 47 (2014).
[3] D. Tong, S. M. Farooqi, J. Stanojevic, S. Krishnan, Y. P. Zhang, R. Côté, E. E. Eyler, and P. L. Gould, Phys. Rev. Lett. **93**, 063001 (2004).
[4] K. Singer, M. Reetz-Lamour, T. Amthor, L. G. Marcassa, and M. Weidemüller, Phys. Rev. Lett. **93**, 163001 (2004).
[5] E. Urban, T. A. Johnson, T. Henage, L. Isenhower, D. D. Yavuz, T. G. Walker, and M. Saffman, Nat. Phys. **5**, 110 (2009).
[6] A. Gaetan, Y. Miroshnychenko, T. Wilk, A. Chotia, M. Viteau, D. Comparat, P. Pillet, A. Browaeys, and P. Grangier, Nat. Phys. **5**, 115 (2009).
[7] M. Saffman, T. G. Walker, and K. Mølmer, Rev. Mod. Phys. **82**, 2313 (2010).
[8] J. D. Pritchard, D. Maxwell, A. Gauguet, K. J. Weatherill, M. P. A. Jones, and C. S. Adams, Phys. Rev. Lett. **105**, 193603 (2010).
[9] S. Sevinçli, N. Henkel, C. Ates, and T. Pohl, Phys. Rev. Lett. **107**, 153001 (2011).
[10] T. Peyronel, O. Firstenberg, Q.-Y. Liang, S. Hofferberth, A. V. Gorshkov, T. Pohl, M. D. Lukin, and V. Vuletic, Nature (London) **488**, 57 (2012).
[11] D. Maxwell, D. J. Szwer, D. Paredes-Barato, H. Busche, J. D. Pritchard, A. Gauguet, K. J. Weatherill, M. P. A. Jones, and C. S. Adams, Phys. Rev. Lett. **110**, 103001 (2013).
[12] H. Weimer, M. Muller, I. Lesanovsky, P. Zoller, and H. P. Buchler, Nat. Phys. **6**, 382 (2010).
[13] H. Labuhn, D. Barredo, S. Ravets, S. de Léséleuc, T. Macrì, T. Lahaye, and A. Browaeys, Nature (London) **534**, 667 (2016).
[14] R. Heidemann, U. Raitzsch, V. Bendkowsky, B. Butscher, R. Löw, L. Santos, and T. Pfau, Phys. Rev. Lett. **99**, 163601 (2007).
[15] J. H. Gurian, P. Cheinet, P. Huillery, A. Fioretti, J. Zhao, P. L. Gould, D. Comparat, and P. Pillet, Phys. Rev. Lett. **108**, 023005 (2012).
[16] I. Mourachko, D. Comparat, F. de Tomasi, A. Fioretti, P. Nosbaum, V. M. Akulin, and P. Pillet, Phys. Rev. Lett. **80**, 253 (1998).
[17] P. Schausz, M. Cheneau, M. Endres, T. Fukuhara, S. Hild, A. Omran, T. Pohl, C. Gross, S. Kuhr, and I. Bloch, Nature (London) **491**, 87 (2012).
[18] G. Günter, H. Schempp, M. Robert-de Saint-Vincent, V. Gavryusev, S. Helmrich, C. S. Hofmann, S. Whitlock, and M. Weidemüller, Science **342**, 954 (2013).

[19] S. Wüster, C. Ates, A. Eisfeld, and J. M. Rost, Phys. Rev. Lett. **105**, 053004 (2010).
[20] S. Möbius, M. Genkin, S. Wüster, A. Eisfeld, and J. M. Rost, Phys. Rev. A **88**, 012716 (2013).
[21] K. Leonhardt, S. Wüster, and J. M. Rost, Phys. Rev. Lett. **113**, 223001 (2014).
[22] P. McQuillen, X. Zhang, T. Strickler, F. B. Dunning, and T. C. Killian, Phys. Rev. A **87**, 013407 (2013).
[23] N. Thaicharoen, A. Schwarzkopf, and G. Raithel, Phys. Rev. A **92**, 040701 (2015).
[24] N. Thaicharoen, L. F. Gonçalves, and G. Raithel, Phys. Rev. Lett. **116**, 213002 (2016).
[25] L. F. Gonçalves, N. Thaicharoen, and G. Raithel, J. Phys. B **49**, 154005 (2016).
[26] R. Faoro, C. Simonelli, M. Archimi, G. Masella, M. M. Valado, E. Arimondo, R. Mannella, D. Ciampini, and O. Morsch, Phys. Rev. A **93**, 030701 (2016).
[27] S. Ichimaru, Rev. Mod. Phys. **54**, 1017 (1982).
[28] J. J. Bollinger and D. J. Wineland, Phys. Rev. Lett. **53**, 348 (1984).
[29] J. H. Chu and Lin I, Phys. Rev. Lett. **72**, 4009 (1994).
[30] D. H. E. Dubin and T. M. O'Neil, Rev. Mod. Phys. **71**, 87 (1999).
[31] C. A. Knapek, A. V. Ivlev, B. A. Klumov, G. E. Morfill, and D. Samsonov, Phys. Rev. Lett. **98**, 015001 (2007).
[32] Ashwin J. and R. Ganesh, Phys. Rev. Lett. **104**, 215003 (2010).
[33] Ashwin J. and R. Ganesh, Phys. Rev. Lett. **106**, 135001 (2011).
[34] G. Bannasch, J. Castro, P. McQuillen, T. Pohl, and T. C. Killian, Phys. Rev. Lett. **109**, 185008 (2012).
[35] J. D. Jackson, *Classical Electrodynamics* (Wiley, New York, 1962).
[36] A. Reinhard, T. C. Liebisch, B. Knuffman, and G. Raithel, Phys. Rev. A **75**, 032712 (2007).
[37] D. Comparat and P. Pillet, J. Opt. Soc. Am. B **27**, A208 (2010).
[38] L. F. Gonçalves and L. G. Marcassa, Phys. Rev. A **94**, 043424 (2016).
[39] J.-P. Hansen and I. R. McDonald, *Theory of Simple Liquids* (Academic, San Diego, 2013).
[40] L. Goldstein and J. Reekie, Phys. Rev. **98**, 857 (1955).
[41] W. E. Massey, Phys. Rev. Lett. **12**, 719 (1964).
[42] E. C. Svensson, V. F. Sears, A. D. B. Woods, and P. Martel, Phys. Rev. B **21**, 3638 (1980).
[43] S. H. Glenzer and R. Redmer, Rev. Mod. Phys. **81**, 1625 (2009).
[44] N. D. Mermin and H. Wagner, Phys. Rev. Lett. **17**, 1133 (1966).
[45] P. C. Hohenberg, Phys. Rev. **158**, 383 (1967).
[46] H. P. Büchler, E. Demler, M. Lukin, A. Micheli, N. Prokof'ev, G. Pupillo, and P. Zoller, Phys. Rev. Lett. **98**, 060404 (2007).
[47] N. Saquet, A. Cournol, J. Beugnon, J. Robert, P. Pillet, and N. Vanhaecke, Phys. Rev. Lett. **104**, 133003 (2010).
[48] L. Wang, H. Zhang, L. Zhang, C. Li, Y. Yang, J. Zhao, G. Raithel, and S. Jia, New J. Phys. **17**, 063011 (2015).
[49] T. Killian, T. Pattard, T. Pohl, and J. Rost, Phys. Rep. **449**, 77 (2007).
[50] G. Bannasch, T. C. Killian, and T. Pohl, Phys. Rev. Lett. **110**, 253003 (2013).
[51] D. Murphy and B. M. Sparkes, Phys. Rev. E **94**, 021201 (2016).
[52] D. R. Nicholson, *Introduction to Plasma Theory* (Wiley, New York, 1983).
[53] J. Hubbard, Proc. R. Soc. London A **260**, 114 (1961).
[54] A. Schwarzkopf, R. E. Sapiro, and G. Raithel, Phys. Rev. Lett. **107**, 103001 (2011).
[55] A. Schwarzkopf, D. A. Anderson, N. Thaicharoen, and G. Raithel, Phys. Rev. A **88**, 061406 (2013).
[56] G. Pupillo, A. Micheli, M. Boninsegni, I. Lesanovsky, and P. Zoller, Phys. Rev. Lett. **104**, 223002 (2010).
[57] F. Maucher, N. Henkel, M. Saffman, W. Królikowski, S. Skupin, and T. Pohl, Phys. Rev. Lett. **106**, 170401 (2011).
[58] T. Macrì and T. Pohl, Phys. Rev. A **89**, 011402 (2014).
[59] I. Bloch, J. Dalibard, and S. Nascimbene, Nat. Phys. **8**, 267 (2012).
[60] K. C. Younge, A. Reinhard, T. Pohl, P. R. Berman, and G. Raithel, Phys. Rev. A **79**, 043420 (2009).